

## Tomography and Purification of the Temporal-Mode Structure of Quantum Light

Vahid Ansari,<sup>1,\*</sup> John M. Donohue,<sup>1,†</sup> Markus Allgaier,<sup>1</sup> Linda Sansoni,<sup>1</sup> Benjamin Brecht,<sup>1,2</sup>

Jonathan Roslund,<sup>3</sup> Nicolas Treps,<sup>3</sup> Georg Harder,<sup>1</sup> and Christine Silberhorn<sup>1</sup>

<sup>1</sup>*Integrated Quantum Optics, Paderborn University, Warburger Strasse 100, 33098 Paderborn, Germany*

<sup>2</sup>*Clarendon Laboratory, Department of Physics, University of Oxford, Parks Road OX1 3PU, United Kingdom*

<sup>3</sup>*Laboratoire Kastler Brossel, Sorbonne Université, CNRS, ENS-PSL Research University, Collège de France; 4 place Jussieu, F-75252 Paris, France*



(Received 26 January 2018; published 23 May 2018)

High-dimensional quantum information processing promises capabilities beyond the current state of the art, but addressing individual information-carrying modes presents a significant experimental challenge. Here we demonstrate effective high-dimensional operations in the time-frequency domain of nonclassical light. We generate heralded photons with tailored temporal-mode structures through the pulse shaping of a broadband parametric down-conversion pump. We then implement a quantum pulse gate, enabled by dispersion-engineered sum-frequency generation, to project onto programmable temporal modes, reconstructing the quantum state in seven dimensions. We also manipulate the time-frequency structure by selectively removing temporal modes, explicitly demonstrating the effectiveness of engineered nonlinear processes for the mode-selective manipulation of quantum states.

DOI: [10.1103/PhysRevLett.120.213601](https://doi.org/10.1103/PhysRevLett.120.213601)

Photons are critical components of quantum networks and technologies, acting as the natural carrier of quantum information due to their low decoherence, simple transmission, and wide range of encoding possibilities. In particular, high-dimensional encodings offer powerful advantages through an increased information-per-photon capacity [1,2], complex entanglement structures [3–6], an enhanced resilience to noise and loss [7,8], and resource-efficient multiuser networking [9]. In order to seize these benefits, single photons in clearly distinguishable, accurately controllable, and practically measurable modes are essential to define a high-dimensional quantum alphabet. The spectral and temporal, or time-frequency, photonic degrees of freedom offer an attractive framework for quantum communication and quantum information processing [10–15]. Unlike polarization and spatial encodings, information encoded in the time-frequency domain is robust through fiber-optic and waveguide transmission, making it a natural candidate for both long-distance quantum communication and compact integrated devices. In particular, broadband temporal modes provide an elegant basis that encodes qudits in intensity-overlapping but field-orthogonal pulses [14]. Because of their pulsed nature, temporal modes lend themselves to network applications relying on the precise synchronization of multiple parties. Additionally, these temporal modes are a natural choice for physical implementations, as they are the eigenbasis of photon pairs emitted from standard parametric down-conversion (PDC) sources [5,16].

To fully exploit the temporal-mode structure of quantum light, it is necessary to both control the modal structure of

quantum light sources and develop matched mode-selective measurement methods. In order to perform projective measurements onto arbitrary temporal modes, techniques are needed which can identify and remove a specific desired mode from a mixture or superposition. Furthermore, operations on photonic temporal modes must not introduce noise in order to leave the fragile quantum nature of the light intact. Sum-frequency generation with tailored group-velocity relationships and shaped ultrafast pulses provides a capable toolbox for these tasks [17–22]. Notably, a sum-frequency process between a weak photonic signal and a shaped strong measurement pulse with matched group velocities has been shown to selectively address individual temporal modes [19,21]. This process, dubbed the quantum pulse gate (QPG), can be used as a temporal-mode analyzer for communication networks [17] or as an add-drop component to build general unitaries and quantum logic gates for a desired temporal-mode basis [14,23]. Recent QPG experiments have shown highly efficient and highly selective operations on coherent light pulses [24–29] and demonstrated its effectiveness as a measurement device for unknown superpositions [30] and as a mode-selective photon subtractor [31]. While some of these works have used weak coherent states [24,26,31], no operations on the temporal modes of genuinely quantum light have been demonstrated to date. In continuous-variable quantum optics, homodyne measurements provide inherently mode-selective detection [5,32–34], but these techniques do not have the add-drop functionality of the QPG and require a knowledge of the underlying photonic quantum state and optical loss to reconstruct the mode distribution.

In this Letter, we show a complete set of tools to generate, measure, and manipulate the temporal-mode structure of single photons with a high degree of control. We orchestrate the modal structure of PDC photon pairs by shaping the pump spectrum. We show that the QPG capably performs projective measurements onto custom temporal modes, with both amplitude and phase sensitivity. We use this functionality to perform a seven-dimensional quantum state tomography of heralded photons and recover their full time-frequency density matrix. We then use the QPG to purify and manipulate the temporal-mode structure of the photons, adjustable through a programmable operation and confirmed through second-order correlation function measurements. We measure high signal-to-noise ratios while operating on quantum light, definitively positioning the QPG as an invaluable resource for pulsed quantum information science.

We generate photon pairs with a variety of underlying modal structures through parametric down-conversion. PDC is a nonlinear process which creates simultaneous signal and idler photons with frequencies  $\omega_s$  and  $\omega_i$ , respectively. The joint spectral amplitude function  $f(\omega_s, \omega_i)$  describes the spectral phase and amplitude of the two-photon state and is determined by the spectral shape of the PDC pump and the dispersive properties of the nonlinear material [16,35–38]. While the joint spectral amplitude contains a complete description of the state in continuous time-frequency space, an equivalent discrete description can be obtained from the Schmidt decomposition [39], which reexpresses it in terms of orthonormal modes with normalized Schmidt coefficients  $\gamma_k$  as

$$f(\omega_s, \omega_i) = \sum_k \sqrt{\gamma_k} \psi_k(\omega_s) \phi_k(\omega_i). \quad (1)$$

For a Gaussian joint spectral amplitude, the eigenmodes are given by Hermite-Gaussian (HG) functions, as sketched in Fig. 1. Notably, these modes have overlapping intensities and therefore cannot be isolated or measured with standard frequency filtering [28].

In this discretized picture, the density matrix  $\rho_{si}$  containing the complete time-frequency description of the two-photon state can be written simply as

$$\rho_{si} = \sum_{i,j} \sqrt{\gamma_i \gamma_j} |\psi_i \phi_i\rangle \langle \psi_j \phi_j|, \quad (2)$$

where  $|\psi_i\rangle$  and  $|\phi_i\rangle$  are the signal and idler photon states, respectively, defined by the corresponding temporal modes. By detecting the idler photon in a time-frequency insensitive manner, the state of the signal photon collapses to  $\rho_s = \sum_i \gamma_i |\psi_i\rangle \langle \psi_i|$ , with a purity of  $P = \text{tr} \rho_s^2 = \sum_i \gamma_i^2$ . In the low-gain regime, the purity is directly related to the second-order autocorrelation function (i.e., the marginal  $g^{(2)}$ ) as  $g^{(2)} = 1 + P$  [40]. This provides an experimentally accessible measure of the underlying modal structure, directly probing the decomposition of the joint spectral amplitude independent of the individual mode shapes.

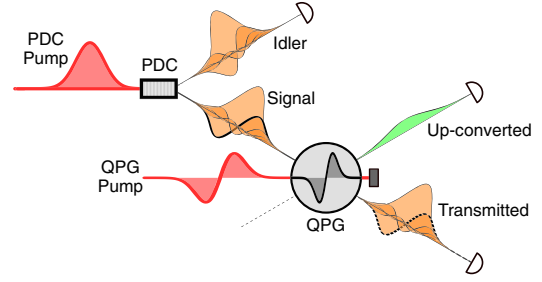


FIG. 1. Temporal-mode selection with a quantum pulse gate. The two-photon state resulting from PDC has a multimode structure defined by the pump field and nonlinear phase matching. The QPG selects a single mode (the first-order Hermite-Gauss, for example, in bold) from this superposition and up-converts it to a higher frequency, while the unselected modes transmit unaffected. Changing the shape of the QPG pump changes which temporal mode the QPG selects.

We implement a mode-selective QPG through sum-frequency generation, a nonlinear process which couples input frequencies  $\omega_{in}$  to output frequencies  $\omega_{out}$ , according to a mapping function  $\xi(\omega_{in}, \omega_{out})$ . This function is given by the product of the complex spectrum of the QPG pump  $\alpha(\omega_{out} - \omega_{in})$  and the phase matching of the material  $\Phi(\omega_{in}, \omega_{out})$ . If the input signal and the QPG pump have the same group velocity, the phase matching can be written as a function of only the output frequency, i.e.,  $\Phi(\omega_{in}, \omega_{out}) \approx \tilde{\Phi}(\omega_{out})$ . For a sufficiently long interaction length, the output frequency range is much narrower than the input [22], and the contribution of the QPG pump spectrum can be approximated as a function of only the input frequency,  $\alpha(\omega_{out} - \omega_{in}) \approx \tilde{\alpha}(\omega_{in})$ . In this limit, the mapping function  $\xi(\omega_{in}, \omega_{out})$  becomes separable, and we can describe the QPG interaction as a single-mode broadband beam splitter coupling an input temporal mode defined by  $\tilde{\alpha}(\omega_{in})$  to the up-converted mode defined by  $\tilde{\Phi}(\omega_{out})$  while transmitting all orthogonal temporal modes unaltered [19,21]. This is schematically depicted for a QPG set to the first-order Hermite-Gauss mode in Fig. 1. By measuring a photon in the up-converted mode, we implement a projective measurement onto a temporal mode that can be freely chosen through standard pulse shaping of the QPG pump [30].

The group-velocity matching condition can be met in periodically poled lithium niobate (PPLN) waveguides, which also provide the spatial confinement necessary for long nonlinear interaction lengths. In our experimental setup, detailed in Supplemental Material [41], we make use of type-II group-velocity matching between a 1540-nm photonic input and an 876-nm QPG pump in a homemade 17-mm PPLN waveguide, as in Refs. [24,30]. We measure up-converted output pulses at 558 nm with a 61-pm (59 GHz) bandwidth (full width at half maximum), significantly narrower than the 4.9-nm (620 GHz) bandwidth of the input photons. Although similar conditions can be met in other materials using near-degenerate processes

[25–27], our scheme avoids the challenge of isolating the single-photon signal from the second harmonic of the QPG pump.

We use spatial-light-modulator-based pulse shapers to define both the spectral amplitude and phase of the PDC and QPG pump pulses [42,43]. With this flexibility in hand, we selected four PDC states to illustrate the versatility of the QPG. The joint spectral intensity  $|f(\omega_s, \omega_i)|^2$  for each is shown on the right side in Fig. 2, as measured with dispersive time-of-flight spectrometers [37,44]. First, we set the PDC pump bandwidth such that the generated two-photon state is nearly spectrally single mode [38], as seen in the nearly separable joint spectral intensity in Fig. 2(a). A singular value decomposition of the joint

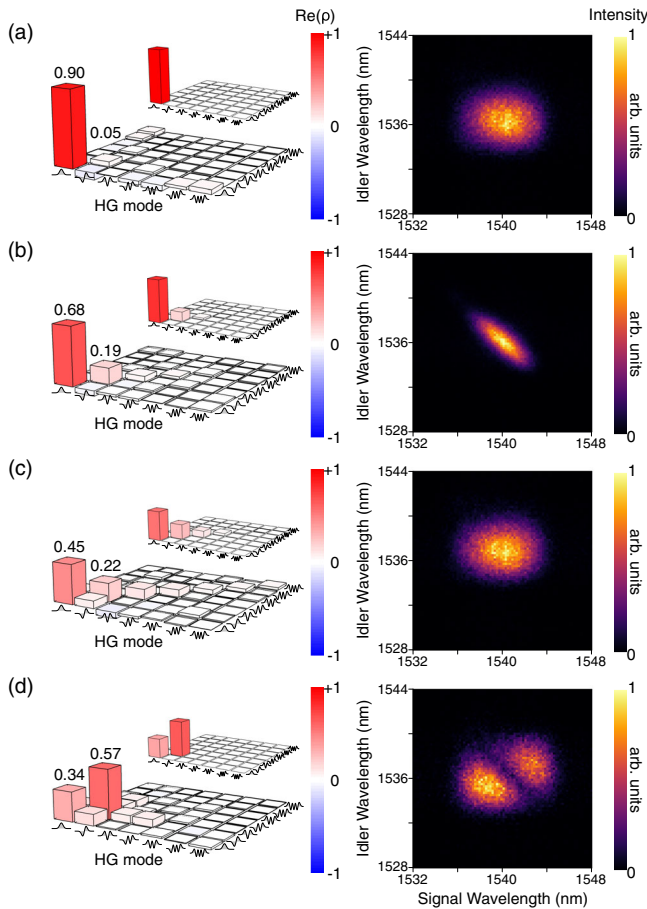


FIG. 2. Joint spectral intensities and reconstructed temporal-mode density matrices. The real part of the seven-dimensional one-photon temporal-mode tomographically reconstructed density matrices (left), joint spectral intensities (right), and theoretically expected density matrices (inset) for four PDC states: (a) a separable PDC state, (b) a PDC state with spectral anticorrelations from a narrow-bandwidth pump, (c) a PDC state with spectral phase correlations from a chirped pump, and (d) a PDC state pumped with a higher-order mode. The values of the first two diagonal entries are explicitly labeled above the density matrix. Imaginary components of the reconstructed density matrices are small and found in Supplemental Material [41].

spectral intensity predicts a purity of 0.995, but the measured  $g^{(2)} = 1 + P$  (corrected for detector dark counts) corresponds to a significantly lower purity of  $0.929 \pm 0.008$ , potentially due to remaining phase correlations or degenerate background processes.

By shaping the QPG pump to project onto a set of Hermite-Gauss spectral shapes, we expect significantly higher up-conversion probabilities for the lowest-order Gaussian mode. We find that, when measuring in coincidence with an idler detection, the Gaussian projection indeed provides more counts than the first-order Hermite-Gaussian projection by a factor of 19.3 (12.8 dB), with an even stronger suppression for higher-order modes. This demonstrates simultaneously the high mode separability of our device and the single-mode character of our PDC state. With a coherent-state input signal from a commercial pulse shaper instead of PDC photons, the suppression factor increases to 111 (20.5 dB). An in-depth characterization of the mode selectivity of this device with classical light can be found in Ref. [30]. The up-converted signal is cleanly separated from all background sources, even for a PDC-generated average photon number of  $\langle n \rangle \approx 0.16$ . The signal-to-noise ratio, including noise from detector dark counts, scattered strong laser light, and competing nonlinear noise processes in the poled waveguide [45], is over 70:1 without heralding and increases to over 900:1 when gated by an idler detection.

While joint spectral intensity measurements provide important information about the two-photon PDC state, they potentially hide significant information about the spectral phase to which mode-selective measurement would be sensitive. To demonstrate the effectiveness of the QPG for quantum state characterization, we reconstruct the density matrix of the signal photons, as seen on the left-hand side in Fig. 2. By shaping the QPG pump, we project onto the first seven Hermite-Gauss temporal modes as well as a tomographically complete set of superpositions, totalling 56 measurements [46,47]. The time-frequency waveforms chosen span eight mutually unbiased seven-dimensional bases and are sketched in Supplemental Material [41]. The density matrices were then reconstructed from the heralded counts in the up-converted mode using a maximum-likelihood approach [48]. As the tomography measurements are made on one photon of a PDC pair, we expect to reconstruct mixed density matrices with purities consistent with the measured  $g^{(2)}$ . For the separable PDC state in Fig. 2(a), we reconstruct a density matrix with a purity of  $\text{Tr}(\rho^2) = 0.896 \pm 0.006$ , lower than the expected value of  $0.929 \pm 0.008$ . Discrepancies between the tomographically reconstructed purities and the  $g^{(2)}$  values arise from the slightly diminished mode selectivity for the higher-order projections [30], to which the characterization of single-mode behavior is particularly sensitive.

Next, we increase the number of modes present in the PDC state in three different ways and show that the QPG measurements are sensitive to all three. First, we narrow the

bandwidth of the PDC pump to produce a multimode PDC state with spectral intensity anticorrelations. The inseparability of this system can be seen directly in the anticorrelations of the joint spectral intensity as well as the additional components of the reconstructed density matrix in Fig. 2(b). The purity of the reconstructed density matrix is found to be  $0.523 \pm 0.008$ , which matches the  $g^{(2)}$ -inferred purity of  $0.528 \pm 0.009$ .

Intensity correlations are not the only available avenue for increasing the mode number of a PDC state. By adding a quadratic spectral phase (chirp) to the PDC pump, we introduce phase correlations between the signal and idler photons. Note that this phase does not affect the joint spectral intensity, as seen in Fig. 2(c). However, the added phase drastically decreases the  $g^{(2)}$ , with a measured purity of  $0.327 \pm 0.005$ . Through tomography, we find that the QPG measurements are also sensitive to this phase, with significantly more diagonal elements in the density matrix and a reconstructed purity of  $0.317 \pm 0.005$ , similar to the  $g^{(2)}$ -inferred purity. This result explicitly demonstrates the limitations of spectral intensity measurements for benchmarking pure single photons and the necessity of spectral phase control. More details on PDC with a chirped pump can be found in Supplemental Material [41].

In each of the previous cases, the primary temporal mode of the PDC state is approximately Gaussian, with higher-order contributions falling off exponentially and no finite cutoff. As a final example, we demonstrate control over the modal composition within a restricted subspace. We produce a state with contributions from principally two temporal modes by shaping the PDC into the first-order Hermite-Gauss function, as seen in Fig. 2(d), which is expected to produce photon pairs in the time-frequency Bell state [14]. The reconstructed density matrix from the QPG measurements shows that the modal content of the PDC state is mainly confined to these two modes, and the purities inferred from the  $g^{(2)}$  and the tomography for this state are, respectively,  $0.498 \pm 0.006$  and  $0.531 \pm 0.004$ , consistent with half of a highly entangled qubit pair. The imbalance between the first two modes can be attributed to a nonideal group-velocity relationship between the signal and idler in the PDC process (i.e., a non-45-degree phase-matching angle [38]) and is consistent with the density matrix expected from the joint spectral intensity.

In addition to being useful as a measurement tool, the QPG in combination with the PDC source can also be used as a source of single-mode photons by isolating one mode from all others [14]. To demonstrate this state purification, we measure the  $g^{(2)}$  of the up-converted photons with the QPG pump in the first two Hermite-Gauss modes, as shown in Fig. 3. If the QPG isolates a single mode from the input mixture, the up-converted photons themselves will be

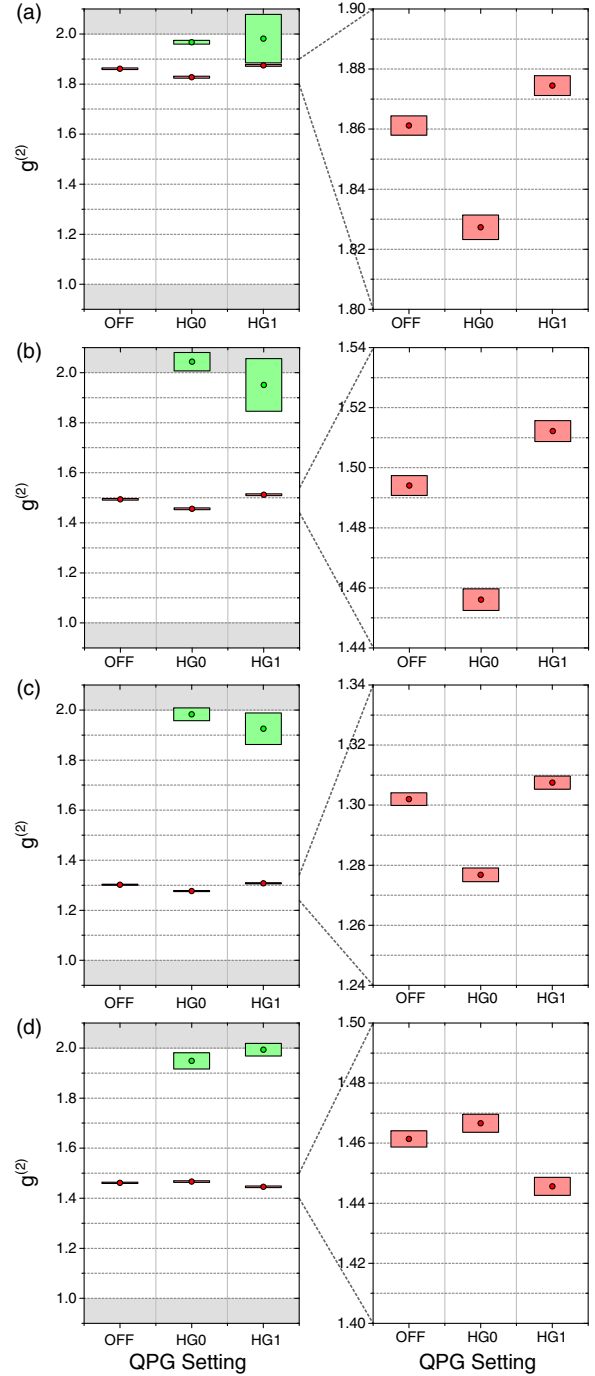


FIG. 3. Second-order autocorrelation functions of transmitted and up-converted photons. The marginal  $g^{(2)}$ 's of the up-converted (green) and transmitted (red) PDC photons are shown for the four PDC states corresponding to Figs. 2(a)–2(d) with the QPG pump pulse delayed relative to the signal photons (“off”) and shaped to the first two Hermite-Gauss temporal modes (“HG0” and “HG1”). The right side of the figure shows the same data rescaled to highlight the changes in the  $g^{(2)}$  of the transmitted photons. The data presented are dark-count background subtracted, and the error bars are found assuming Poissonian noise.

highly pure. Indeed, the  $g^{(2)}$  of the up-converted light confirms a purity of at least 0.9 for both the zeroth- and first-order HG modes, regardless of the PDC state under interrogation. For example, for the correlated spectral intensity of case (b), the  $g^{(2)}$  of the up-converted light when the Gaussian mode is selected is  $1.95 \pm 0.04$ , which increases to  $2.04 \pm 0.04$  after dark-count subtraction. The purity of the up-converted light remains high when the first-order HG mode is selected. The high  $g^{(2)}$  values measured here conclusively show both that the QPG indeed selects a single mode and that the up-converted mode retains the thermal photon statistics of PDC, with very little noise introduced by the process.

Finally, we show through the  $g^{(2)}$  that the modal structures of the transmitted photons are significantly altered by the QPG. If a mixture of modes is dominated by one mode, partially removing that mode from the mixture will increase the mixedness of the remaining distribution, akin to the Procrustean method of entanglement concentration [49]. For the decorrelated PDC state of case (a), we measured the conversion efficiency through the depletion of the transmitted signal as approximately 22%, limited by the nonlinear interaction strength and the available QPG pump power. This partial removal of the primary mode indeed results in a significant decrease in the  $g^{(2)}$  of the unconverted transmitted signal photons, as seen on the right-hand side in Fig. 3, consistent with the efficiency measured from the input depletion. Conversely, removing the first-order HG mode removes amplitude from the secondary Schmidt coefficient, which increases the relative amplitude of the primary Schmidt mode. This is seen in cases (a)–(c) to increase the overall purity of the transmitted photon state, demonstrating that the QPG can act as a temporal mode cleaner even for the nonconverted photons. In case (d), the first-order HG mode is present in a larger proportion than the Gaussian component, and the opposite trend is seen. This result directly demonstrates that the QPG can be used to remove modal components from a single-photon state. QPG efficiencies above 80% have been demonstrated with classical light [24,26,27], and schemes to reach unit efficiency have been shown with double-pass configurations [29,50], which combined with this result pave the way for mode-selective add or drop functionality.

We have shown that the quantum pulse gate can be used to directly manipulate and measure the temporal modal structure of single-photon states. By projecting over a complete set of temporal modes and superpositions, we reconstructed seven-dimensional temporal-mode density matrices for PDC photons with a variety of modal structures. We have demonstrated that the output of the pulse gate is nearly completely purified regardless of the input, positioning the quantum pulse gate as a powerful tool for photonic quantum state engineering. We have also demonstrated through changes in the second-order auto-correlation function that the quantum pulse gate modifies

the modal structure of the input photons, establishing the QPG as a novel device for both entanglement concentration and state purification. Future work will focus on improving the efficiency and extending the accessible dimensionality of the quantum pulse gate to fully realize its potential for time-frequency mode-selective measurement, as a conversion interface and add or drop device for temporally encoded quantum networks, and as a platform for high-dimensional quantum state characterization.

We thank T. Bartley, D. V. Reddy, and J. Tiedau for fruitful discussions. This research has received funding from the Deutsche Forschungsgemeinschaft (DFG) via Sonderforschungsbereich TRR 142, the Gottfried Wilhelm Leibniz-Preis, and from the European Unions (EU) Horizon 2020 Research and Innovation program under Grant Agreement No. 665148. J.M.D. gratefully acknowledges support from Natural Sciences and Engineering Resource Council of Canada (NSERC).

\* vahid.ansari@uni-paderborn.de

† john.matthew.donohue@uni-paderborn.de

- [1] J. Leach, E. Bolduc, D. J. Gauthier, and R. W. Boyd, *Phys. Rev. A* **85**, 060304 (2012).
- [2] T. Zhong *et al.*, *New J. Phys.* **17**, 022002 (2015).
- [3] M. Agnew, J. Leach, M. McLaren, F. S. Roux, and R. W. Boyd, *Phys. Rev. A* **84**, 062101 (2011).
- [4] S. Yokoyama, R. Ukai, S. C. Armstrong, C. Sornphiphathphong, T. Kaji, S. Suzuki, J.-I. Yoshikawa, H. Yonezawa, N. C. Menicucci, and A. Furusawa, *Nat. Photonics* **7**, 982 (2013).
- [5] J. Roslund, R. M. De Araujo, S. Jiang, C. Fabre, and N. Treps, *Nat. Photonics* **8**, 109 (2014).
- [6] C. Reimer *et al.*, *Science* **351**, 1176 (2016).
- [7] N. J. Cerf, M. Bourennane, A. Karlsson, and N. Gisin, *Phys. Rev. Lett.* **88**, 127902 (2002).
- [8] T. Vértesi, S. Pironio, and N. Brunner, *Phys. Rev. Lett.* **104**, 060401 (2010).
- [9] I. Herbauts, B. Blauensteiner, A. Poppe, T. Jennewein, and H. Huebel, *Opt. Express* **21**, 29013 (2013).
- [10] W. Tittel, J. Brendel, H. Zbinden, and N. Gisin, *Phys. Rev. Lett.* **81**, 3563 (1998).
- [11] J. Mower, Z. Zhang, P. Desjardins, C. Lee, J. H. Shapiro, and D. Englund, *Phys. Rev. A* **87**, 062322 (2013).
- [12] J. Nunn, L. J. Wright, C. Söller, L. Zhang, I. A. Walmsley, and B. J. Smith, *Opt. Express* **21**, 15959 (2013).
- [13] J. M. Lukens, A. Dezfouliyan, C. Langrock, M. M. Fejer, D. E. Leaird, and A. M. Weiner, *Phys. Rev. Lett.* **112**, 133602 (2014).
- [14] B. Brecht, D. V. Reddy, C. Silberhorn, and M. G. Raymer, *Phys. Rev. X* **5**, 041017 (2015).
- [15] S. Schwarz, B. Bessire, A. Stefanov, and Y.-C. Liang, *New J. Phys.* **18**, 035001 (2016).
- [16] A. B. U'Ren, C. Silberhorn, R. Erdmann, K. Banaszek, W. P. Grice, I. A. Walmsley, and M. G. Raymer, *Laser Phys.* **15**, 146 (2005).
- [17] Z. Zheng and A. Weiner, *Opt. Lett.* **25**, 984 (2000).

- [18] A. Pe'er, B. Dayan, A. A. Friesem, and Y. Silberberg, *Phys. Rev. Lett.* **94**, 073601 (2005).
- [19] A. Eckstein, B. Brecht, and C. Silberhorn, *Opt. Express* **19**, 13770 (2011).
- [20] J. M. Donohue, M. Agnew, J. Lavoie, and K. J. Resch, *Phys. Rev. Lett.* **111**, 153602 (2013).
- [21] D. V. Reddy, M. G. Raymer, C. J. McKinstrie, L. Mejling, and K. Rottwitt, *Opt. Express* **21**, 13840 (2013).
- [22] M. Allgaier, V. Ansari, L. Sansoni, C. Eigner, V. Quiring, R. Ricken, G. Harder, B. Brecht, and C. Silberhorn, *Nat. Commun.* **8**, 14288 (2017).
- [23] B. Brecht, A. Eckstein, A. Christ, H. Suche, and C. Silberhorn, *New J. Phys.* **13**, 065029 (2011).
- [24] B. Brecht, A. Eckstein, R. Ricken, V. Quiring, H. Suche, L. Sansoni, and C. Silberhorn, *Phys. Rev. A* **90**, 030302 (2014).
- [25] A. S. Kowligy, P. Manurkar, N. V. Corzo, V. G. Velez, M. Silver, R. P. Scott, S. J. B. Yoo, P. Kumar, G. S. Kanter, and Y.-P. Huang, *Opt. Express* **22**, 27942 (2014).
- [26] P. Manurkar, N. Jain, M. Silver, Y.-P. Huang, C. Langrock, M. M. Fejer, P. Kumar, and G. S. Kanter, *Optica* **3**, 1300 (2016).
- [27] D. V. Reddy and M. G. Raymer, *Opt. Express* **25**, 12952 (2017).
- [28] A. Shahverdi, Y. M. Sua, L. Tumei, and Y.-P. Huang, *Sci. Rep.* **7**, 6495 (2017).
- [29] D. V. Reddy and M. G. Raymer, *Optica* **5**, 423 (2018).
- [30] V. Ansari, G. Harder, M. Allgaier, B. Brecht, and C. Silberhorn, *Phys. Rev. A* **96**, 063817 (2017).
- [31] Y.-S. Ra, C. Jacquard, A. Dufour, C. Fabre, and N. Treps, *Phys. Rev. X* **7**, 031012 (2017).
- [32] C. Polycarpou, K. N. Cassemiro, G. Venturi, A. Zavatta, and M. Bellini, *Phys. Rev. Lett.* **109**, 053602 (2012).
- [33] Z. Qin, A. S. Prasad, T. Brannan, A. MacRae, A. Lezama, and A. Lvovsky, *Light Sci. Appl.* **4**, e298 (2015).
- [34] J. Tiedau, V. Shchesnovich, D. Mogilevtsev, V. Ansari, G. Harder, T. Bartley, N. Korolkova, and C. Silberhorn, *New J. Phys.* **20**, 033003 (2018).
- [35] W. P. Grice and I. A. Walmsley, *Phys. Rev. A* **56**, 1627 (1997).
- [36] O. Kuzucu, M. Fiorentino, M. A. Albota, F. N. C. Wong, and F. X. Kaertner, *Phys. Rev. Lett.* **94**, 083601 (2005).
- [37] T. Gerrits *et al.*, *Opt. Express* **19**, 24434 (2011).
- [38] G. Harder, V. Ansari, B. Brecht, T. Dirmeier, C. Marquardt, and C. Silberhorn, *Opt. Express* **21**, 13975 (2013).
- [39] C. K. Law, I. A. Walmsley, and J. H. Eberly, *Phys. Rev. Lett.* **84**, 5304 (2000).
- [40] A. Christ, K. Laiho, A. Eckstein, K. N. Cassemiro, and C. Silberhorn, *New J. Phys.* **13**, 033027 (2011).
- [41] See Supplemental Material at <http://link.aps.org/supplemental/10.1103/PhysRevLett.120.213601> for detailed experimental methods.
- [42] A. M. Weiner, *Rev. Sci. Instrum.* **71**, 1929 (2000).
- [43] A. Monmayrant, S. Weber, and B. Chatel, *J. Phys. B* **43**, 103001 (2010).
- [44] M. Avenhaus, A. Eckstein, P. J. Mosley, and C. Silberhorn, *Opt. Lett.* **34**, 2873 (2009).
- [45] J. S. Pelc, L. Ma, C. Phillips, Q. Zhang, C. Langrock, O. Slattery, X. Tang, and M. M. Fejer, *Opt. Express* **19**, 21445 (2011).
- [46] W. K. Wootters and B. D. Fields, *Ann. Phys. (N.Y.)* **191**, 363 (1989).
- [47] S. Bandyopadhyay, P. O. Boykin, V. Roychowdhury, and F. Vatan, *Algorithmica* **34**, 512 (2002).
- [48] J. B. Altepeter, E. R. Jeffrey, and P. G. Kwiat, *Adv. At. Mol. Opt. Phys.* **52**, 105 (2005).
- [49] C. H. Bennett, H. J. Bernstein, S. Popescu, and B. Schumacher, *Phys. Rev. A* **53**, 2046 (1996).
- [50] D. V. Reddy, M. G. Raymer, and C. J. McKinstrie, *Opt. Lett.* **39**, 2924 (2014).